AIAA 93-0903
Aerodynamic Effects on Primary Breakup of Turbulent Liquids

P.-K. Wu and G. M. Faeth
Department of Aerospace Engineering
The University of Michigan
Ann Arbor, MI

31st Aerospace Sciences Meeting & Exhibit
January 11-14, 1993 / Reno, NV

AIAA-93-0903

AERODYNAMIC EFFECTS ON PRIMARY BREAKUP OF TURBULENT LIQUIDS

P.-K. Wu* and G. M. Faeth†
Department of Aerospace Engineering
The University of Michigan, Ann Arbor, Michigan 48109-2140

Abstract

An experimental study of primary breakup of turbulent liquids is described, emphasizing liquid/gas density ratios less than 500 where aerodynamics effects are important. The experiments involved multiphase mixing layers along round water jets (3.6 and 6.2 mm dia.) injected at various velocities into still helium, air and Freon 12 at pressures of 1 and 2 atm. with fully-developed turbulent pipe flow at the jet exit. Pulsed shadowgraph photography and holography were used to find conditions at the onset of breakup as well as drop properties as a function of distance from the jet exit. Two main aerodynamic effects were observed, as follows: (1) enhanced primary breakup near the onset of breakup, and (2) merged primary and secondary breakup when the Rayleigh breakup times of ligaments formed by turbulent fluctuations were longer than the secondary breakup times of similar sized drops. The predictions of phenomenological theories based on these ideas were in good agreement with the measurements.

NOMENCLATURE

C_s = empirical constant for SMD after secondary breakup
C_{sa} = empirical constant for enhanced breakup
C_{si} = empirical constant for SMD at onset of breakup
C_{sx} = empirical constant for SMD variation with x
C_{xi} = empirical constant for x at onset of breakup
d = injector diameter
d_{max},d_{min} = maximum and minimum image dimensions of drops
d_p = drop diameter
e_p = volume-averaged ellipticity
ℓ = characteristic eddy size
ℓ_K = Kolmogorov length scale
L_c = liquid core length
L = Rayleigh breakup length
MMD = mass median drop diameter
Oh_d = Ohnesorge number, $\mu_f/(\rho_f d\sigma)^{1/2}$
p = pressure
r = radial distance
Re_{ij} = Reynolds number base on phase i and length scale j, $\bar{u}_{oj}j/\nu_i$
SMD = Sauter mean diameter
SMD_p = SMD after primary breakup for a merged primary and secondary breakup
u = streamwise velocity
u_p = streamwise drop velocity
v = radial velocity
v_ℓ = radial velocity associated with eddy of size ℓ
v_p = radial drop velocity
We_{ij} = Weber number based on phase i and length scale j, $\rho_i\bar{u}_o^2 j/\sigma$
x = streamwise distance
Λ = radial integral length scale
μ = molecular viscosity
ν = kinematic viscosity
ρ = density
σ = surface tension
τ_b = characteristic secondary breakup time
τ_R = characteristic Rayleigh breakup time

Subscripts
f = liquid-phase property
g = gas-phase property
i = at point of breakup initiation
o = jet exit condition

Superscripts
$\bar{(\ )}$ = time-averaged mean property
$\tilde{(\ )}$ = mass-averaged mean property
$(\ )'$ = time-averaged r.m.s. fluctuating property

INTRODUCTION

An experimental study of aerodynamic effects on the primary breakup of turbulent liquids is described, extending earlier work on the primary breakup of nonturbulent liquids,[1] and on the primary breakup of turbulent liquids at conditions where aerodynamic effects were small.[2] The research is motivated by the importance of primary breakup to the structure and mixing properties of sprays and other dispersed multiphase flows, in view of the potential for significant aerodynamic effects on primary breakup at the high pressures of many practical applications.[3] Similar to Ref. 2, the experiments involved conditions near the surface of round liquid jets in still gases, with fully-developed turbulent pipe flow at the jet exit. The measurements included properties at the location of the onset of turbulent primary breakup as well as drop sizes and velocities resulting from primary breakup as a function of distance from the jet exit. Additionally, phenomenological theories were developed to help interpret and correlate the measurements, extending the methods of Ref. 2 to include aerodynamic phenomena.

Many investigators have observed significant effects of liquid turbulence on the structure and mixing properties of pressure atomized sprays in still gases.[4-14] In general, liquid turbulence enhances mixing rates and yields larger drops after primary breakup at the liquid surface than nonturbulent liquid jets at comparable conditions. Wu et al.[1] studied the primary breakup of turbulent liquids at liquid/gas density ratios greater than 500, finding that turbulent primary breakup largely was controlled by liquid turbulence properties with negligible aerodynamic effects at these conditions. Thus, successful phenomenological theories (non-aerodynamic turbulent primary breakup theories) for both the onset and for drop properties after turbulent primary breakup were developed by treating interactions between surface tension and liquid turbulence properties alone.[2] Subsequent measurements at liquid/gas density ratios less than 500, however, yielded drop

* Research Fellow.
† Professor, Fellow AIAA.

sizes that were significantly smaller than the non-aerodynamic turbulent primary breakup predictions and evidence that the appearance of aerodynamic effects was governed by the liquid/gas density ratio alone.[4] Nevertheless, only limited information about aerodynamic turbulent primary breakup was reported in Ref. 4, prompting the present more detailed study of the phenomenon.

The paper begins with a description of experimental methods. Results are then considered treating flow visualization, drop size distributions and velocities after primary breakup, the onset of primary breakup and the variation of drop sizes after primary breakup with distance from the jet exit, in turn. The paper concludes with a discussion of the regimes of non-aerodynamic and aerodynamic turbulent primary breakup. Present considerations were limited to injection of water into various gases to obtain ρ_f/ρ_g in the range 104-6230, because effects of liquid type had been examined earlier.[1]

EXPERIMENTAL METHODS

Apparatus

The apparatus involved liquid injection into still gases within a windowed chamber. A sketch of the test arrangement appears in Fig. 1. The injector was modified somewhat from earlier work,[1,2] to accommodate operation in the windowed test chamber. It consisted of a pneumatically driven piston/cylinder arrangement containing a roughly 600 ml water sample. The outlet of the cylinder was rounded to prevent cavitation and was followed by constant diameter passages having length-to-diameter ratios greater than 41, to yield nearly fully-developed turbulent pipe flow at the jet exit.[8] Jet passage diameters of 3.6 and 6.2 mm were considered during the tests. Injection was vertically downward with the liquid collected in the bottom of the chamber and then discarded.

The windowed test chamber was cylindrical with a diameter of 300 mm and a length of 1370 mm. The chamber could be evacuated and refilled with various gases at pressures of 1 and 2 atm. to provide variations of the liquid/gas density ratio while avoiding problems of injector cavitation at low pressures. The instrumentation was mounted rigidly; therefore, various distances from the jet exit were considered by traversing the injector with respect to the chamber in the vertical direction while horizontal positions were varied by traversing the entire injector and chamber assembly.

The piston/cylinder arrangement was filled with water by venting the upper side of the cylinder and temporarily plugging the exit of the jet passage. Water was then admitted to the portion of the accumulator below the piston, forcing the piston upward and filling the sample volume. Once the chamber was full, the water flow was ended and the plug at the passage exit removed. Test operation was then initiated by admitting high-pressure air to the upper side of the piston through a solenoid valve which forced the liquid through the jet passage. Similar to earlier work,[1,2] total times of injection were short, 270-4000 ms, however, these times were sufficient due to short flow development and data acquisition times. Jet exit velocities at the time of the measurements were calibrated with an impact plate as described in Ref. 2.

Instrumentation

The instrumentation consisted of pulsed shadowgraph photography and pulsed holography. The following descriptions of these systems will be brief, see Refs. 1 and 2 for more details.

Photography. Pulsed shadowgraph photography was used to measure flow properties near the onset of breakup where dispersed-phase concentrations were relatively low so that this approach is feasible. This provided better resolution than pulsed holography to improve observations in the region where the smallest drops were observed. The holocamera was used for these photographs, operating in the single-pulse mode with the reference beam blocked to yield a shadowgraph rather than a hologram. Image analysis to find drop sizes was the same as the holography measurements to be discussed next.

Pulsed shadowgraph photography also was used to find the streamwise location of the onset of turbulent primary breakup. The experimental uncertainties (95% confidence) of breakup locations were less than 40%, which is relatively large due to the angular variation of the direction of ligaments protruding from the surface and the randomness of drops separating from the tips of ligaments.

Holography. The double-pulse holocamera and reconstruction systems were similar to past work.[1, 2, 4, 6, 7] The hologram image itself had a 5-6:1 primary magnification so that the reconstruction optics allowed drop diameters as small as 5 μm to be observed. The holocamera could be double pulsed with pulse separation times as small as 1 μs to allow drop velocities to be measured. The reconstructed images were analyzed with a Gould FD 5000 image display system having a field of view of 1.4 × 1.6 mm. Various locations in the reconstructed image could be observed by traversing the hologram to change the streamwise and radial position, and the video camera of the display system to change the tangential position.

For consistency, drop sizes and velocities were found in the same manner as past work.[1, 2, 4, 6, 7] Small drops were sized by measuring their maximum and minimum diameters through the centroid of their image. Then, assuming an ellipsoidal shape, the drop diameter was defined as the diameter of a sphere having the same volume, i.e., $d_p^3 = d_{min}^2\, d_{max}$. The shape of the drop was characterized by its ellipticity, i.e., $e_p = d_{max}/d_{min}$. More irregular objects, where the centroid was outside the projected image of the object, were sized by finding the area and perimeter of the image and proceeding as before for an ellipsoidal having the same area and perimeter. Measurements at each condition were summed over 40-200 objects to provide drop size distributions, the mass median diameter (MMD), the Sauter mean diameter (SMD) and the volume averaged ellipticity, e_p. Experimental uncertainties of these properties were dominated by finite sampling limitations because primary breakup, particularly near the onset of breakup, yields relatively few drops. Within the limitations of the definitions of object sizes and ellipticities, experimental uncertainties (95% confidence) are estimated to be less than 40% for MMD, SMD and e_p.

Object velocities were based on the motion of the centroid of the image using holocamera pulses of different intensity to resolve directional ambiguity. Similar to object sizes, 40-200 objects were measured to find mass-weighted (Favre) averaged drop velocities. Experimental uncertainties (95% confidence) were dominated by finite sampling limitations, and are estimated to be less than 20% for $\tilde{u}_p$ and less than 60% for the much smaller values of $\tilde{v}_p$.

Test Conditions

The overall data base included present measurements as well as those from Refs. 2, 4 and 7 for turbulent primary breakup. The operating conditions for these tests are

summarized in Table 1. Using water as the injected liquid, with gas environments of helium, air and Freon 12 at pressures of 1 and 2 atm., liquid/gas density ratios in the range 104-6230 were obtained. Injector diameters of 3.6, 6.2 and 9.5 mm were studied in order to vary the integral scales of the turbulence; these arrangements had injector passage length-to-diameter ratios of 210, 121 and 41, respectively, all of which are sufficient to provide nearly fully-developed turbulent pipe flow at the jet exit.[8,15] The streamwise and radial integral scales of the turbulence at the jet exit were taken to be 0.4 d and d/8, respectively, based on the measurements of Laufer for fully-developed turbulent pipe flow cited by Hinze.[16]

The streamwise positions of the present measurements included x/d in the range 0.2-60. Earlier work[11,13,14] indicated that the length of the liquid core was in excess of x/d = 100 for present conditions which agrees with present observation of surfaces at all test conditions. Thus, present experiments involve primary breakup at the liquid surface rather than conditions after breakup of the entire liquid volume itself.

Jet exit velocities were in the range 22-67 m/s, yielding the following ranges of jet and primary breakup dynamic parameters: Re_{fd} of 90,000-500,000, We_{gd} of 12-3790, We_{fd} of 60,000-390,000 and Oh_d of 0.0011-0.0018. All test conditions where aerodynamic effects were observed involved air and Freon 12 as the ambient gas, with $We_{fd} > 8$ and $We_{gd} > 40$. This places them in the atomization breakup regime for nonturbulent liquids defined by Miesse[17] and Ranz,[18] where primary breakup should begin right at the jet exit. Actually, the onset of primary breakup always occurred at some distance from the jet exit as will be discussed later in more detail. The present low values of Oh_d imply that viscosity should not play a major role in the breakup of the flow as a whole,[3] although it does affect the smallest scales of the turbulence,[15,16] and the properties of secondary breakup[19] that interact with primary breakup,[15] as discussed later.

RESULTS AND DISCUSSION

Flow-Visualization

Consideration of the results will begin with visualization of the flow in order to provide an overview of the nature of aerodynamic effects on the turbulent primary breakup process. Similar visualizations, showing effects of varying the distance from the jet exit, and the velocity of the liquid, are presented in Refs. 2 and 8 for conditions where aerodynamic effects are not a factor. These results show that drop sizes after turbulent primary breakup roughly correspond to the sizes of ligaments and other protrusions from the liquid surface. Additionally, the sizes of surface protrusions, and corresponding drops, progressively increase with increasing distance from the jet exit for a given injection condition. This behavior was attributed to two effects.[2] First of all, small disturbances complete their growth faster than large disturbances and should be observed sooner. Secondly, reduced levels of turbulence production as liquid velocities become uniform, once the retarding effect of the injector passage walls is removed, cause the liquid turbulence to decay with the small-scale high wave number range of the turbulence, and the corresponding distortion of the liquid surface, disappearing first. An observation supporting small aerodynamic effects for the conditions of Ref. 2 was that liquid protuberances were more-or-less randomly oriented with respect to the liquid surface, thus exhibiting little effect of drag forces from the gas. The main effect of velocity increases for these conditions was to reduce the size of the smallest scale disturbances while leaving the large scale disturbances relatively unchanged at a particular x/d. This behavior was attributed to the properties of the power spectrum of the turbulence, where for a particular flow configuration, increasing velocities (Reynolds numbers) do not modify integral scales appreciably but do increase the kinetic energy available to distort the liquid surface at high wave numbers.[2,8,21] These qualitative observations were supported by phenomenological theories based on these ideas that yielded reasonable agreement with measurements.[2]

Some typical pulsed shadowgraph photographs for the present test conditions are illustrated in Fig. 2. These results all are for water injection with d = 3.6 mm, $\bar{u}_o$ = 38 m/s and x/d = 10. The gas environments for these observations, however, were changed to highlight aerodynamic effects and consisted of still helium, air and Freon 12 at atmospheric pressure (from left to right), to provide ρ_f/ρ_g = 6230, 867 and 213, respectively. The direction of liquid motion in the photographs is vertically downward, which corresponds to the orientation of the experiment although effects of gravitational forces were negligible due to the high liquid velocity. The liquid core of the jet is toward the left of each photograph. Finally, a 900 μm diameter pin is visible in all three photographs in order to provide a size reference.

The photographs of Fig. 2 illustrate some of the main features of aerodynamic phenomena on turbulent primary breakup. First of all, it is evident from the left and center photographs that varying ρ_f/ρ_g from 6230 to 867 has virtually no effect on properties near the liquid surface, even though a density ratio change of this magnitude might be expected to influence aerodynamic forces on protrusions from the surface and drops near the surface. In particular, ligament properties and drop sizes and concentrations are essentially the same for these two conditions, while the orientation of ligaments protruding from the surface is random. This behavior is reasonable, however, because estimated velocity variations of ligament sized objects over the residence time of the ligaments is small at these density ratios.[2] Thus, primary breakup properties and the mass fluxes of liquid entering the dispersed phase depend on liquid turbulence properties rather than aerodynamic breakup and stripping at these conditions.[2]

The lowest density ratio condition shown in Fig. 2, however, exhibits rather different behavior from the other two conditions. First of all, drop sizes are smaller and drop number densities are higher near the liquid surface for the low density ratio condition. This is a clear indication of the aerodynamic effects anticipated as ρ_f/ρ_g decreases, because all other properties of the flows are the same. The smaller drop sizes provide evidence of aerodynamic stripping of drops from ligaments which has been called merged primary and secondary breakup in Refs. 2 and 4. The larger number densities of drops are then reasonable due to the breakup of larger liquid elements. Rates of aerodynamic stripping of liquid from the surface are proportional to $(\rho_f/\rho_g)^{-1/2}$ which also should contribute to larger liquid volume fractions and thus more drops near the liquid surface.[22-24] In particular, decreasing liquid/gas density ratios below 500 has been observed to enhance the mixing rates of turbulent liquid jets in gases.[5]

Other features of the photograph in Fig. 2 at the lowest liquid/gas density ratio support the presence of significant aerodynamic effects at this condition as well. For example, the ligaments generally are deflected toward the jet exit, as anticipated when drag forces are more significant, rather than the random orientations seen at the two higher density ratios. Furthermore, there is a tendency for the ligaments to be shorter

at the lowest liquid/gas density ratio, which is consistent with effects of aerodynamic stripping of drops from their tips, i.e., merged primary and secondary breakup.

Another factor that suggested the appearance of aerodynamic effects for liquid/gas density ratios less than roughly 500, was the tendency for the onset of turbulent primary breakup to progressively move toward the jet exit as ρ_f/ρ_g was decreased in this regime. In contrast, the position of the onset of turbulent primary breakup was essentially independent of ρ_f/ρ_g when this ratio was greater than 500.[2] This behavior of the onset of turbulent primary breakup will be taken up quantitatively, after the properties of drop size distributions and drop velocities after primary breakup have been considered.

Drop Size Distributions

Drop size distributions after turbulent primary breakup were measured for all the test conditions. It was found that the size distribution functions agreed with Simmons'[25] universal root normal distribution with the ratio MMD/SMD = 1.2 within experimental uncertainties. This behavior agrees with earlier measurements of drop size distributions after nonturbulent and turbulent primary breakup[1,2] as well as with drop size distributions near the surface and across the mixing layer in regions of dense sprays where the liquid core still is present,[4,6,7] all of which yield MMD/SMD = 1.2 within similar experimental uncertainties. The root normal distribution only has two moments; therefore, taking the best estimate of MMD/SMD = 1.2 implies that the entire drop size distribution is known if the SMD is known. Thus, drop sizes will be described in terms of the SMD alone in the following, similar to past work.[1,2,4,6,7]

Drop Velocities

In order to help contrast the properties of non-aerodynamic and aerodynamic turbulent primary breakup, drop velocities after primary breakup will be considered next. Available measurements of volume (mass) averaged streamwise and crosstream drop velocities, both normalized by $\bar{u}_o$, are plotted as a function of x/d in Fig. 3. The measurements include all the test conditions summarized in Table 1. Results for $\rho_f/\rho_g < 500$ are shown as darkened and half darkened symbols, while results for $\rho_f/\rho_g > 500$ are shown as open symbols, in order to highlight the properties of the low liquid/gas density ratio regime where aerodynamic effects are thought to be important.

The normalized drop velocities illustrated in Fig. 3 provide crude correlations in terms of x/d but other factors probably are involved, as well. Near the jet exit, $\tilde{u}_p/\bar{u}_o$ has a value of near 0.6 which increases to roughly 0.9 for x/d > 20. This behavior is consistent with drop velocities after turbulent primary breakup being roughly the same as streamwise liquid velocities near the liquid surface. The lower streamwise velocities are expected near the jet exit due to the retarding effect of the passage wall, evolving to higher values farther downstream where liquid velocities become more uniform.[2] Superimposed on this behavior, however, is a clear trend that measurements for $\rho_f/\rho_g < 500$ have significantly lower mean streamwise velocities than the higher density ratio conditions — on the average roughly 20-40% lower. This can be attributed to aerodynamic drag if it is recalled that gas velocities near the liquid surface tend to be relatively low because the dispersed-phase region is very dilute (liquid volume fractions are less than 0.1%) so that momentum transfer to the gas phase is not very effective and separated-flow effects are large.[4,6,7] Then, recent measurements of mass averaged drop velocity changes during secondary breakup of 20-40%,[20] are consistent with similar reductions of streamwise drop velocities during present observations for conditions where aerodynamic effects are significant.

Similar trends with respect to density variations are much less clear for the crosstream velocity component, $\tilde{v}_o'/\bar{u}_o$ in Fig. 3. In general, crosstream drop velocities are comparable to crosstream velocity fluctuations in the liquid similar to past observations.[2] In particular maximum values of $v_o'/\bar{u}_o = 0.058$ for fully-developed turbulent pipe flow,[15,16] even in the region near the wall, which is comparable to the results seen in Fig. 3 in view of the large experimental uncertainties and scatter of this velocity component. An explanation of why the crosstream velocity component does not exhibit a reduction due to drag at low values of ρ_f/ρ_g, similar to the streamwise velocity component, is provided by an aerodynamic effect other than drag. In particular, the classical aerodynamic theories of primary drop breakup are based on the idea that flow velocities in the radial direction are increased for protuberances from the liquid surface due to acceleration of the gas over the tip of the protuberance,[22,24] see the sketch appearing in Fig. 4. This yields a radial pressure drop across the protuberance which should increase the radial velocities of drops near the surface when aerodynamic effects are significant. This mechanism would tend to compensate for drag effects in the radial direction during merged primary and secondary breakup. Thus, it is plausible that radial drop velocities are not significantly changed in the presence of aerodynamic effects within the rather large scatter of the measurements. Thus, the observations of Figs. 2 and 3 appear to be consistent with estimates of observable variations of the velocities of ligaments and large drops due to aerodynamic effects over the time period of primary breakup for ρ_f/ρ_g less than 500.[4]

Onset of Breakup

The properties of the onset of turbulent primary breakup will be considered next. The properties of interest include drop sizes formed at the onset of breakup and the distance from the jet exit where breakup begins. Conditions for turbulent primary breakup to occur at all can be inferred from these results, based on distances from the jet exit required for the onset of turbulent primary breakup that exceed estimates of the length of the liquid core itself. Estimates of liquid core lengths needed for this purpose can be found from past work in the literature,[3,11-14] and will not be considered here. The onset problem will be addressed by extending the approach of Ref. 2, where the onset of breakup was associated with conditions where the momentum of turbulent fluctuations in the liquid was sufficient to overcome surface tension forces so that drops could form, to include aerodynamic contributions. Both the drop sizes at the onset of breakup, and the location where breakup begins, will be considered in the following.

Drop Sizes at Onset. Phenomenological analysis to find drop properties at the onset of breakup will be based on the configuration illustrated in Fig. 4. This implies that the onset of breakup for present test conditions did not involve merged primary and secondary breakup, which is plausible due to relatively long secondary breakup times at onset conditions,[19] as discussed later. Thus, the onset mechanism is assumed to involve the formation of a drop from a turbulent eddy having a characteristic size, ℓ, and a characteristic

crosstream velocity relative to the surrounding liquid, v_{ℓ}. The eddy is shown with an elongated shape because length scales in the streamwise direction are larger than in the crosstream direction for turbulent pipe flow.[15,16] The eddy is assumed to be convected in the streamwise direction at the local mean velocity, which is taken to be $\bar{u}_o$ based on the results discussed in connection with Fig. 3. The drop formed by the eddy also is assumed to have a diameter comparable to ℓ.

Drops formed at the onset of turbulent primary breakup are the smallest drops that can be formed by this mechanism.[2] The smallest drops that can be formed are either comparable to the smallest or Kolmogorov scales of turbulence, ℓ_K, or the smallest eddy that has sufficient mechanical energy to provide the surface energy needed to form a drop — whichever is larger. For present test conditions, ℓ_K was in the range 1-10 μm, which is much smaller than the smallest observed drop sizes; therefore, only the second criterion will be considered here, even though the first criterion may be relevant for some applications.

The second criterion for the smallest drop that can be formed can be found from energy considerations. The mechanical energy available to form a drop includes the kinetic energy of an eddy of characteristic size, ℓ_i, relative to its surroundings, plus the added mechanical energy due to the pressure drop caused by acceleration of the surrounding gas over the tip of the protuberance, as illustrated in Fig. 4. Equating these sources of mechanical energy to the surface energy required to form a drop then yields:

$$(\rho_f v_{\ell i}^2 + C_{sa} \rho_g \bar{u}_o^2) \ell_i^3 = C_{si} \sigma \ell_i^2 \qquad (1)$$

where various factors associated with surfaces, volumes, etc., have been absorbed in the empirical coefficients C_{sa} and C_{si}. These coefficients also include effects of ellipticity, nonuniform velocities within the eddy, nonuniform pressure variations over surfaces of the protuberance, and the efficiency of conversion of mechanical energy into surface energy. Equation (1) is similar to the expression used in Ref. 2, except for the addition of the second term on the left hand side of the equation which represents the aerodynamic enhancement of the mechanical energy available for the primary breakup process. In order for drops to be formed at all, ℓ_i must be less than the largest eddies present, which are comparable to Λ [16], while $\ell_K < \ell_i$ by definition for this primary breakup mechanism. Then it is reasonable to assume that ℓ_i is in the inertial range of the turbulence spectrum, which implies:[21]

$$v_{\ell i} \sim \bar{v}_o' (\ell_i/\Lambda)^{1/3} \qquad (2)$$

where variations of turbulence properties in the liquid have been ignored, similar to Ref. 2. Combining Eqs. (1) and (2), setting $SMD_i \sim \ell_i$, and assuming that turbulence properties in the liquid can be approximated by jet exit turbulence properties, yields the following implicit equation for SMD_i:

$$\frac{SMD_i}{\Lambda} \left(1 + C_{sa} \left(\frac{\rho_g}{\rho_f}\right) \left(\frac{\bar{u}_o}{\bar{v}_o'}\right)^2 \left(\frac{\Lambda}{SMD_i}\right)^{2/3}\right)^{3/5} = C_{si} \left(\frac{\bar{u}_o}{\bar{v}_o'}\right)^{6/5} We_{f\Lambda}^{-3/5} \qquad (3)$$

where the new proportionality constants have been absorbed into C_{sa} and C_{si} as before. With fully-developed turbulent pipe flow at the jet exit, $\bar{v}_o'/\bar{u}_o$ is essentially a constant.[15,16] Thus, the effect of the aerodynamic enhancement term in Eq. (3) is largely controlled by the liquid/gas density ratio, yielding a non-aerodynamic regime at large ρ_f/ρ_g that was explored in Ref. 2, and an aerodynamic regime at small ρ_f/ρ_g where SMD_i depends on the liquid/gas density ratio. This helps support past observations that the onset of aerodynamic effects depend on the liquid/gas density ratio rather than dynamic properties related to the liquid velocity.[2,4]

Present measurements of SMD_i are plotted in terms of the variables of Eq. (3) in Fig. 5. In doing this, C_{sa} was optimized to a value of 0.04, based on taking $\bar{v}_o'/\bar{u}_o = 0.058$ for fully-developed turbulent pipe flow.[16] In addition to present results, measurements from Ref. 2 also are shown on the plot, which involve a variety of liquids for conditions where aerodynamic effects are not important. As before, test conditions for $\rho_f/\rho_g < 500$, where aerodynamic effects are observed, are denoted by darkened and half-darkened symbols, while tests at $\rho_f/\rho_g > 500$, where aerodynamic effects could not be identified, are shown as open symbols. The correlation of the data for all conditions generally is within the scatter anticipated from experimental uncertainties. The power of $We_{f\Lambda}$ from the correlation of the data is not -3/5 as suggested by Eq. (3), however, and can be represented better by the following empirical fit that is shown on the plot:

$$\frac{SMD_i}{\Lambda} \left(1 + 0.04 \left(\frac{\rho_g}{\rho_f}\right) \left(\frac{\bar{u}_o}{\bar{v}_o'}\right)^2 \left(\frac{\Lambda}{SMD_i}\right)^{2/3}\right)^{3/5} = 76\, We_{f\Lambda}^{-0.69} \qquad (4)$$

The standard deviations of the coefficient and power in Eq. (4) are 9 and 6%, respectively, and the correlation coefficient of the fit is 0.97. Thus, the reduction of the power of $We_{f\Lambda}$ from -3/5 in Eq. (3) to -0.69 in Eq. (4) is not statistically significant within the uncertainties of the fit, and certainly in view of the approximations used to develop the correlation. Additionally, Eq. (4) agrees within 10% with the expression developed in Ref. 2 for the regime where $\rho_f/\rho_g > 500$. The coefficient of Eq. (4) is relatively large but this is anticipated from Eq. (3) because $(\bar{u}_o/\bar{v}_o')^{6/5}$ is large for fully-developed pipe flow, e.g., $C_{si} = 2.5$ based on the $\bar{v}_o'/\bar{u}_o$ ratio used before, which is order unity as expected for a parameter of this type.

Location of Onset. Given SMD_i, the approach to find the location of the onset of turbulent primary breakup, x_i, is similar to Ref. 2. To find x_i, it is assumed that the drop-forming eddy convects along the liquid surface with a streamwise velocity, $\bar{u}_o$, based on the results of Fig. 3. Then

$$x_i = \bar{u}_o \tau_i \qquad (5)$$

where τ_i is the time required for an eddy of characteristic size, ℓ_i, to form a drop. The aerodynamic enhancement effect will be ignored when finding τ_i, assuming that the aerodynamic pressure drop mainly allows primary breakup to occur for smaller characteristic eddy sizes, rather than modifying the breakup mechanism of protrusions or ligaments. In addition, it is assumed that the onset of breakup is not due to merged primary and secondary breakup for present conditions, similar to considerations used to find SMD_i. Then, the time for growth of ligaments until their breakup into drops is taken to be the Rayleigh breakup time, which is the shortest characteristic breakup time for onset of primary breakup conditions, following Ref. 2.

Considering Rayleigh breakup for a protruding ligament of diameter ℓ_i and jetting velocity $v_{\ell i}$, the breakup length, L_i, of the liquid column, or ligament, is:[26]

$$L_i/\ell_i \sim (\rho_f \ell_i v_{\ell i}^2/\sigma)^{1/2} + 3\mu_f v_{\ell i}/\sigma \qquad (6)$$

For present conditions, the second term on the right hand side of Eq. (6) is small and will be ignored, although it could be a factor for very viscous liquids, i.e., for conditions where the Ohnesorge number based on ℓ_i is not small. Then assuming that τ_i is proportional to the time required for a ligament to grow to its breakup length, $L_i/v_{\ell i}$, τ_i becomes:

$$\tau_i \sim (\rho_f \ell_i^3/\sigma)^{1/2} \qquad (7)$$

Substituting Eq. (7) into Eq. (6), and letting $SMD_i \sim \ell_i$ as before, then yields:

$$x_i/\Lambda \sim (SMD_i/\Lambda)^{3/2} We_{f\Lambda}^{1/2} \qquad (8)$$

The results of Eq. (8) show that drop sizes increase with increasing distance from the jet exit for onset conditions, supporting the idea that onset involves the smallest drops that can be formed. Finally, substituting Eq. (3) for SMD_i into Eq. (8) and rearranging yields the following expression for x_i:

$$\frac{x_i}{\Lambda}\left(1 + C_{sa}\left(\frac{\rho_g}{\rho_f}\right)\left(\frac{\bar{u}_o}{\bar{v}_o'}\right)^2\left(\frac{\Lambda}{SMD_i}\right)^{2/3}\right)^{9/10}$$

$$= C_{xi}\left(\frac{\bar{u}_o}{\bar{v}_o'}\right)^{9/5} We_{f\Lambda}^{-4/10} \qquad (9)$$

where C_{xi} is a constant of proportionality. Similar to Eq. (3), aerodynamic effects on x_i from Eq. (9) are controlled by the liquid/gas density ratio alone, in agreement with present and earlier,[2,4] observations.

Both the present measurements of x_i, and those of Ref. 2, are plotted in terms of the variables of Eq. (9) in Fig. 6, adopting $C_{sa} = 0.04$ as before. Conditions where aerodynamic effects are significant are denoted by darkened and half-darkened symbols, similar to Figs. 3 and 5. The correlation of the data over the full range of aerodynamic effects is reasonably good in view of the relatively large experimental uncertainties of x_i. As before, however, the power of $We_{f\Lambda}$ for the correlation of the data is not -0.4 as suggested by the Eq. (9), but can be represented better by the following empirical expression which is shown on the plot:

$$\frac{x_i}{\Lambda}\left(1 + 0.04\left(\frac{\rho_g}{\rho_f}\right)\left(\frac{\bar{u}_o}{\bar{v}_o'}\right)^2\left(\frac{\Lambda}{SMD_i}\right)^{2/3}\right)^{9/10}$$

$$= 2570\, We_{f\Lambda}^{-0.63} \qquad (10)$$

The standard deviation of the coefficient and power on the right hand side of Eq. (10) are 8 and 10%, respectively, while the correlation coefficient of the fit is 0.89. Thus, the difference between the powers of $We_{f\Lambda}$ in Eqs. (9) and (10) is statistically significant but is not large in view of the approximations used to develop the correlating expression. The large value of the coefficient of Eq. (10) can be anticipated from Eq. (9) because $(\bar{u}_o/\bar{v}_o')^{9/5}$ is a large number for fully-developed turbulent pipe flow, e.g., taking $\bar{v}_o'/\bar{u}_o = 0.058$ as before, yields $C_{sx} = 12$.

A useful expression relating x_i and SMD_i can be obtained by combining the phenomenological results of Eqs. (3) and (9) to yield:

$$x_i/\Lambda = (C_{xi}/C_{si}^{3/2})\,(SMD_i/\Lambda)^{3/2}\, We_{f\Lambda}^{1/2} \qquad (11)$$

Equation (11) is the same as the analogous result when aerodynamic effects are not important,[2] because breakup times and distances were assumed to be uninfluenced by aerodynamic phenomena through Eqs. (5) and (7), i.e., aerodynamic effects only were assumed to allow smaller drops to form at the onset of turbulent primary breakup. Carrying out the same exercise for the best fit correlations of Eqs. (4) and (10) yields:

$$x_i/\Lambda = 3.88\,(SMD_i/\Lambda)^{3/2}\, We_{f\Lambda}^{0.41} \qquad (12)$$

Equation (12) is seen to be consistent with Eq. (11); namely, the coefficient is of order unity while the power of $We_{f\Lambda}$ is not statistically different than 1/2 based on the standard deviations of the powers of the empirical fits.

Drop Sizes

Aerodynamic secondary breakup times scale as $\tau_i \sim \ell_i (\rho_f/\rho_g)^{1/2}/\bar{u}_o$ for an object of size ℓ_i, if the velocity of the gas near the liquid surface is assumed to be small.[19,27] Thus, for conditions where aerodynamic effects are important, Rayleigh breakup times from Eq. (7) increase more rapidly than secondary breakup times as ℓ_i increases. This implies a tendency for secondary and primary breakup to merge as distance from the jet exit increases — a mechanism that dominated drop sizes near the liquid surface for present test conditions, except near the onset of turbulent primary breakup. The configuration considered during the present analysis is illustrated in Fig. 7; namely, that a drop of characteristic size ℓ forms by the turbulent primary breakup mechanism and immediately undergoes secondary breakup to yield a number of smaller drops.

Within the merged primary and secondary breakup regions, turbulent primary breakup properties will be found using the results of Ref. 2 while aerodynamic secondary breakup properties will be found using the results of Ref. 19. The variation of SMD with distance from the jet exit for turbulent primary breakup was found assuming that the SMD was proportional to the largest drop that could be formed at a particular position with the time of breakup determined from the Rayleigh breakup time.[2] Thus, this approach was similar to the approach just described in connection with the onset of breakup. This yields the following expression for the variation of SMD with distance from the jet exit,[2] analogous to Eq. (11):

$$SMD_p/\Lambda = C_{sx}[x/(\Lambda\, We_{f\Lambda}^{1/2})]^{2/3} \qquad (13)$$

The secondary breakup correlation of Ref. 19 was developed assuming that relative velocities at the time of breakup can be represented by the initial relative velocity and that drop sizes after breakup are proportional to the thickness of liquid boundary layers that form within the drop due to gas motion over its secondary surface. This yields the following expression for the SMD after aerodynamic secondary breakup of a drop of diameter d_p having a relative velocity $\bar{u}_o$,[19] assuming that the jet exit velocity is the appropriate relative velocity for merged primary and secondary breakup:

$$SMD/d_p = C_s(\rho_f/\rho_g)^{1/2}(\mu_f/(\rho_f d_p \bar{u}_o))^{1/2} \quad (14)$$

Then assuming that $d_p \sim SMD_p$, Eqs. (13) and (14) can be combined to yield the following expression for the SMD after merged primary and secondary breakup:

$$\rho_g SMD\, \bar{u}_o^2/\sigma = C_s C_{sx}^{1/2} (x/\Lambda)^{1/3} (\rho_g/\rho_f)^{3/4} We_{f\Lambda}^{5/6} Re_{f\Lambda}^{-1/2} \quad (15)$$

where C_s in Eq. (15) is modified from Eq. (14) to account for a range of initial drop sizes rather than a single drop.

Present measurements of aerodynamic turbulent primary breakup, along with some results from Ref. 4, are plotted according to the variables of Eq. (15) in Fig. 8. The following best fit correlation of present measurements also is shown on the plot.

$$\rho_g SMD\, \bar{u}_o^2/\sigma = 12.0\,[(x/\Lambda)^{1/3} (\rho_g/\rho_f)^{3/4} We_{f\Lambda}^{5/6} Re_{f\Lambda}^{-1/2}]^{1.17} \quad (16)$$

where the standard deviation of the coefficient and power on the right-hand-side of Eq. (16) are 2 and 8%, respectively, with a correlation coefficient of 0.92 of the fit. Additionally, adopting the best fit values of C_s and C_{sx} in Eq. (15), the following theoretical prediction for SMD as a function of distance is obtained:

$$\rho_g SMD\, \bar{u}_o^2/\sigma = 12.9\,(x/\Lambda)^{1/3} (\rho_g/\rho_f)^{3/2} We_{f\Lambda}^{5/6} Re_{f\Lambda}^{-1/2} \quad (17)$$

with the standard deviation of the constant of 21%. Thus, the differences between Eqs. (16) and (17) are not statistically significant, within experimental uncertainties. Present measurements also are in good agreement with the predictions. However, the measurements of Tseng et al.[4] definitely yield smaller drop sizes after merged primary and secondary breakup. An explanation of this behavior is that these flows involved the highest concentrations of drops after turbulent primary breakup of the data base, so that drop properties near the liquid surface could be influenced by small drops migrating from other parts of the multiphase mixing layer by turbulent dispersion.

The consistency of the merged primary and secondary breakup process also can be examined by inverting the process; namely, by computing the drop sizes that should have been observed after primary breakup in the absence of aerodynamic effects and comparing these results with other measurements at similar conditions. To do this, the non-aerodynamic turbulent primary breakup correlation was refitted to find C_{sx} in Eq. (13), based on present measurements in helium and air, along with initial breakup results for Freon 12. This yielded

$$SMD/\Lambda = 0.65\,[\,x/(\Lambda\, We_{f\Lambda}^{1/2})\,]^{2/3} \quad (18)$$

with the standard deviation of the coefficient of 34% and a 95% confidence interval of 0.60-0.71. This implies reasonably consistent measurements of turbulent primary breakup with respect to Ref. 2 where the constant of Eq. (18) was 0.64. Then from the fit of the measurements illustrated in Fig. 8, the relationship between SMD and SMD_p is given by:

$$SMD_p/\Lambda = 3.91 \times 10^{-3} (\rho_g/\rho_f)^{1/2} Re_{f\Lambda} (SMD/\Lambda)^2 \quad (19)$$

The results illustrated in Fig. 8, where primary and secondary breakup occurred, were inverted to get SMD_p using Eq. (19). These results are plotted in Fig. 9, along with previous results for turbulent primary breakup where aerodynamic effects are not important from Ref. 2. Aside from the few results of Ref. 4, mentioned earlier in connection with Fig. 8, the inverted aerodynamic turbulent primary breakup measurements are seen to be in good agreement with the other results, supporting the idea of merging of primary and secondary breakup. Other features of this figure, including the liquid core length of Grant and Middleman[11] shown on the plot, are discussed in Ref. 2.

Breakup Regimes

Present measurements suggested three regimes of turbulent primary breakup: (1) non-aerodynamic turbulent primary breakup; (2) aerodynamically-enhanced turbulent primary breakup, observed at onset conditions; and (3) aerodynamic turbulent primary breakup, which involves merging of turbulent primary and secondary breakup. The results also indicated that the liquid/gas density ratio, and the relative magnitudes of characteristic Rayleigh breakup times of ligaments and secondary breakup times of liquid objects, fixed *the boundaries of these regimes. The breakup times used to* define these regimes were based on the SMD after primary breakup, or after the primary breakup stage of merged primary and secondary breakup, for conditions beyond the onset of breakup for present data. Then by analogy to Eq. (7), the characteristic Rayleigh breakup time was taken to be $\tau_R \sim (\rho_f SMD^3/\sigma)^{1/2}$. Similarly, by analogy to the results of Ref. 19 and 27, the characteristic secondary breakup time was taken to be, $\tau_R \sim (\rho_f/\rho_g)^{1/2} SMD/\bar{u}_o$. Then using Eq. (18) to eliminate SMD from the ratio, the characteristic time ratio was taken to be:

$$\tau_R/\tau_b = (\rho_g/\rho_f)^{1/2}(x\, We_{f\Lambda}/\Lambda)^{1/3} \quad (20)$$

The resulting turbulent primary breakup regimes based on present measurements, as well as those from Refs. 2, 4 and 7, are illustrated in terms of ρ_f/ρ_g and τ_R/τ_b in Fig. 10. The results yield the following criteria for transitions between regimes:

$\rho_f/\rho_g = 500$, non-aerodynamic/aerodynamic transition (21)

$\tau_R/\tau_b = 4$, merged/enhanced-aerodynamic transition (22)

In the non-aerodynamic breakup regime, the results of Ref. 2 can be used to find properties at the onset of turbulent primary breakup, and the subsequent variation of SMD with distance from the jet exit; or with similar accuracy, within experimental uncertainties, Eqs. (4) and (9) can be used to find onset properties and Eq. (18) to find the subsequent variation of SMD with x. Otherwise, onset conditions that fall in the enhanced- aerodynamic breakup regime are provided by Eqs. (4) and (9), while the subsequent variation of SMD with x in the merged aerodynamic breakup regime is given by Eq. (17).

DISCUSSION

The present results suggest that most of the features of turbulent primary breakup — conditions at the onset of breakup and the variation of SMD with distance after breakup begins — can be explained by interactions among liquid turbulence, Rayleigh breakup of ligaments and fast (merged) secondary breakup. Additionally, the classical aerodynamic effect that causes a reduced pressure over protuberances from the surface,[21,23] appears to play a role in reducing drop sizes near onset conditions of turbulent primary breakup when liquid/gas density ratios are less than 500. Furthermore, the rather close correspondence between effects of secondary breakup on the primary breakup process observed here, and

secondary breakup of drops exposed to shock wave disturbances observed in Refs. 19 and 20, helps support the relevance of the latter measurements to practical spray processes. However, it still remains to be seen whether slower subsequent variations of drop properties, causing drops to again cross secondary breakup limits within a developing spray flow field, can also be handled successfully in the same manner.

It also should be noted that several features of turbulent primary breakup have not been addressed due to limitations of the available data base. This includes onset in the merged aerodynamic breakup regime, SMD variations with distance in the enhanced aerodynamic breakup regime, turbulent primary breakup limited by the Kolmogorov scales of the turbulence, liquid turbulence properties other than fully-developed turbulent pipe flow, and turbulent primary breakup involving significant effects of liquid viscosity (large Ohnesorge number effects), among others. Additionally, more work is needed to provide better definition of the breakup regime boundaries illustrated in Fig. 10, aside from potential effects due to the phenomena that just were enumerated. Finally, primary breakup near the tip of the liquid core still must be addressed along with the potential for merged primary and secondary breakup in this region. In view of the importance of primary breakup to the subsequent properties of sprays, these issues clearly merit additional study.

CONCLUSIONS

Aerodynamic effects on primary breakup within the multiphase mixing layer of the near jet-exit region of large-scale pressure-atomized sprays were studied, considering liquid jets in still gases with fully-developed turbulent pipe flow at the jet exit. The major conclusions of the study are as follows:

1. The presence of aerodynamic phenomena for turbulent primary breakup largely is controlled by the liquid/gas density ratio, and affect both conditions at the onset of breakup, and drop sizes and velocities (to a lesser extent) after breakup, when this ratio is less than 500. Within this region, regimes of enhanced aerodynamic breakup and merged primary and secondary breakup also were observed (cf. Fig. 10).

2. Aerodynamic enhancement of the onset of turbulent primary breakup was due to the aerodynamic pressure reduction over the tips of protruding liquid elements. This effect assists the kinetic energy of a corresponding liquid eddy relative to its surrounding to provide the surface tension energy needed to form a drop, thus allowing smaller drops to form. Phenomenological analysis based on these ideas yielded reasonable correlations of onset properties, Eqs. (4) and (9), for the enhanced aerodynamic breakup regime (cf. Figs. 5 and 6).

3. For conditions where secondary breakup times become small in comparison to Rayleigh breakup of turbulence-induced ligaments protruding from the surface, processes of turbulent primary and secondary breakup merge yielding smaller drops than when aerodynamic effects are absent. The reduction of drop sizes at these conditions correlated reasonably well with results for the secondary breakup of drops due to shock disturbances from Ref. 19, yielding the correlation of Eq. (17) (cf. Fig. 8).

4. Drop size distributions after aerodynamic turbulent primary breakup approximated Simmons'[25] universal root normal distribution with MMD/SMD = 1.2, similar to observations of other drop breakup processes as well as drops in the multiphase mixing layers of pressure-atomized sprays.[1-8,19,20] Additionally, mass-averaged drop velocities after aerodynamic turbulent primary breakup approximate mean and rms velocity fluctuations of the liquid in the streamwise and crosstream directions, respectively, although there was a tendency for streamwise velocities to be somewhat reduced by aerodynamic effects (cf. Fig. 3).

Present results are limited to liquids having moderate viscosities at conditions where the SMD at the onset of breakup is at least an order of magnitude greater than Kolmogorov length scales with fully-developed turbulent pipe flow at the jet exit. Effects of changes of these conditions, as well as other issues mentioned in the Discussion, merit further study due to the importance of primary breakup to the structure and dynamics of practical sprays.

ACKNOWLEDGEMENTS

This research was sponsored by the Office of Naval Research Grant N00014-89-J-1199 under the Technical Management of G. D. Roy. Initial development of the instrumentation was sponsored by the Air Force Office of Scientific Research, Grant No. 89-0516 with J. M. Tishkoff serving as Technical Manager. The U.S. Government is authorized to reproduce and distribute copies for governmental purposes notwithstanding any copyright notation thereon.

REFERENCES

[1]P.-K. Wu, G.A.Ruff, and G.M. Faeth, "Primary Breakup in Liquid/Gas Mixing Layers," Atomization and Sprays, Vol. 1, 1991, pp. 421-440.

[2]P.-K. Wu, L.-K. Tseng, and G.M. Faeth, "Primary Breakup in Gas/Liquid Mixing Layers for Turbulent Liquids," Atomization and Sprays, Vol. 2, 1992, pp. 295-317.

[3]G.M. Faeth, "Structure and Atomization Properties of Dense Turbulent Sprays," *Twenty-Third Symposium (International) on Combustion*, The Combustion Institute, Pittsburgh, 1990, pp. 1345-1352.

[4]L.-K. Tseng, P.-K. Wu, and G.M. Faeth, "Dispersed-Phase Structure of Pressure-Atomized Sprays at Various Gas Densities," J. Prop. Power, in press.

[5]L.-K. Tseng, G.A. Ruff, and G.M. Faeth, "Effects of Gas Density on the Structure of Liquid Jets in Still Gases," AIAA J., Vol. 30, 1992, pp. 1537-1544.

[6]G.A. Ruff, P.-K. Wu, L.P. Bernal, and G.M. Faeth, "Continuous- and Dispersed-Phase Structure of Dense Nonevaporating Pressure-Atomized Sprays," J. Prop. Power, Vol. 8, 1992, pp. 280-289.

[7]G.A. Ruff, L.P. Bernal, and G.M. Faeth, "Structure of the Near-Injector Region of Non-Evaporating Pressure-Atomized Sprays," J. Prop. Power, Vol. 7, 1991, pp. 221-230.

[8]G.A. Ruff, A.D. Sagar, and G.M. Faeth, "Structure and Mixing Properties of Pressure-Atomized Sprays," AIAA J., Vol. 27, 1989, pp. 901-908.

[9]K. J. DeJuhasz, O. F. Zahm, Jr., and P.H. Schweitzer, "On the Formation and Dispersion of Oil Sprays," Bulletin No. 40, Engineering Experiment Station, The Pennsylvania State University, University Park, PA, 1932, pp. 63-68.

[10]D.W. Lee, and R.C. Spencer, "Photomicrographic Studies of Fuel Sprays," NACA Report No. 454, 1933.

[11]R.P. Grant, and S. Middleman, "Newtonian Jet Stability," AIChE J., Vol. 12, 1966, pp. 669-678.

[12]R.E. Phinney, "The Breakup of a Turbulent Jet in a Gaseous Atmosphere," J. Fluid Mech., vol. 88, 1966, pp. 119-127.

[13]H. Hiroyasu, M. Shimizu, and M. Arai, "The Breakup of a High Speed Jet in a High Pressure Gaseous Environment," University Of Wisconsin, Madison, WI, ICLASS-82, 1982.

[14]B. Chehroudi, Y. Onuma, S.-H. Chen, and F. V. Bracco, "On the Intact Core of Full Cone Sprays," SAE Paper No. 850126, 1985.

[15]H. Schlichting, *Boundary Layer Theory*, 7th ed., McGraw-Hill, New York, p. 599, 1979.

[16]J. O. Hinze, *Turbulence*, 2nd ed., McGraw-Hill, New York, pp. 427 and 724-742, 1975.

[17]C.C. Miesse, "Correlation of Experimental Data on the Disintegration of Liquid Jets," Ind. Engr. Chem., Vol. 47, 1955. pp. 1690-1697.

[18]W.E. Ranz, "Some Experiments on Orifice Sprays," Can. J. Chem. Engr., Vol. 36, 1958, pp. 175-181.

[19]L.-P.Hsiang, and G.M. Faeth, "Near-Limit Drop Deformation and Secondary Breakup," Int. J. Multiphase Flow, Vol. 19, 1992, pp. 635-652.

[20]L.-P. Hsiang, and G. M. Faeth, "Drop Size and Velocity Distributions Following Secondary Breakup," AIAA Paper No. 93-0000, 1993.

[21]H. Tennekes, and J.L. Lumley, *A First Course in Turbulence*, M.I.T. Press, Cambridge, Massachusetts, 1972,pp. 248-286.

[22]G.I. Taylor, "Generation of Ripples by Wind Blowing over a Viscous Liquid," *The Scientific Papers of Sir Geoffrey Ingram Taylor*, Vol. III, G.K. Batchelor, ed., Cambridge Univ. Press, Cambridge, England, 1963, pp. 244-254.

[23]V.G. Levich, *Physicochemical Hydrodynamics*, Prentice-Hall, Inc., Englewood Cliffs, NJ, 1962, pp. 639-646.

[24]R.D. Reitz, and F.V. Bracco, "Mechanism of Atomization of a Liquid Jet," Phys. Fluids, Vol. 25, 1982, pp. 1730-1742.

[25]H.C. Simmons, "The Correlation of Drop-Size Distributions in Fuel Nozzle Sprays," J. Engr. for Power, Vol. 99, 1977, pp. 309-319.

[26]C. Weber, "Zum Zerfall eines Flussigkeitsstrahles," Z. Angewesen. Math. Mech., Vol. 2, 1931, pp. 136-141.

[27]A.A. Ranger, and J.A. Nicholls, "The Aerodynamic Shattering of Liquid Drops," AIAA J., Vol. 7, 1969, pp. 285-290.

Table 1 Summary of Test Conditions[a]

Gas	Helium	Air	Air[b,c]	Air[c]	Freon 12
ρ_g (kg/m^3)	0.16	1.15	1.15	2.34,4.68	4.68,9.63
ρ_f/ρ_g	6230	867	867	213,426	104,213
d (mm)[c]	3.6,6.2	3.6,6.2	9.5	9.5	3.6,6.2
u_o (m/s)	30-67	30-47	21-47	40	22-67
$Re_{fd} \times 10^{-4}$	15-46	15-46	22-50	42	9-46
We_{gd}	12-63	84-452	70-350	502,1005	115-3790
$We_{fd} \times 10^{-4}$	7-39	7-39	6-30	21	7-39
$Oh_d \times 10^3$	1.4,1.8	1.4,1.8	1.1	1.1	1.4,1.8

[a]Pressure-atomized injection of water vertically downward in still gases at 298 ± 3 K with fully-developed turbulent pipe flow at the jet exit. Passage length-to-diameter ratios of 210, 121 and 41 for d = 3.6, 6.2 and 9.5 mm, respectively.
[b]From Ruff et al.[7]
[c]From Tseng et al.[4]

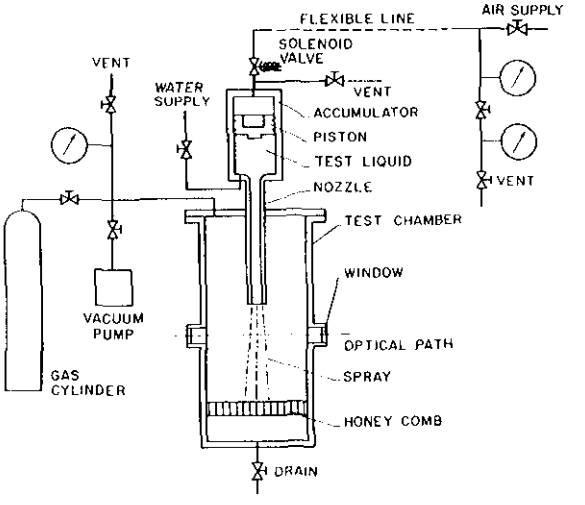

Fig. 1 Sketch of the experimental apparatus.

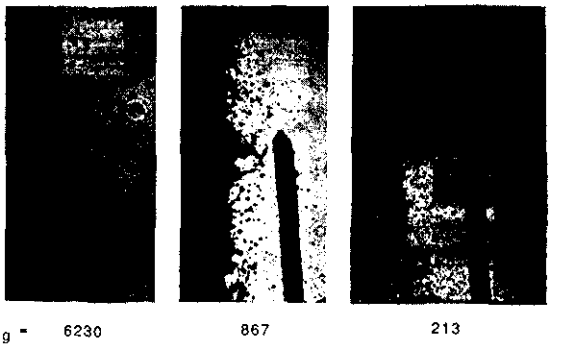

Fig. 2 Pulsed shadowgraphs of turbulent primary breakup in different gas environments: d = 3.6 mm, $\bar{u}_o$ = 38 m/s and x/d = 10 with ρ_f/ρ_g = 6230 (left), 867 (center) and 213 (right).

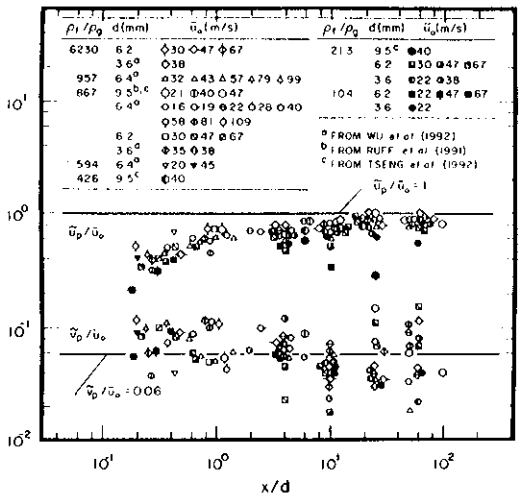

Fig. 3 Mass-averaged drop velocities after breakup as a function of distance from the jet exit.

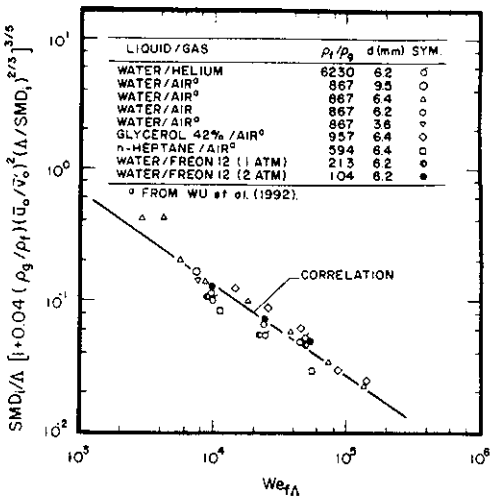

Fig. 5 SMD at the initiation of aerodynamically-enhanced turbulent primary breakup as a function of $We_{f\Lambda}$. The correlation is from Eq. (4).

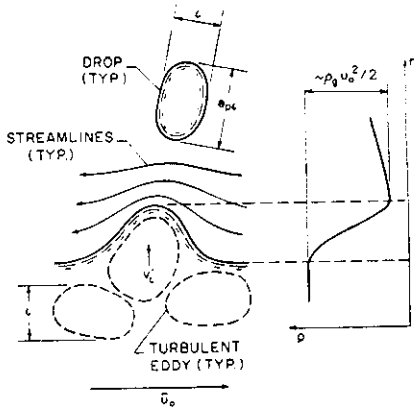

Fig. 4 Sketch of aerodynamically-enhanced turbulent primary breakup at the liquid surface.

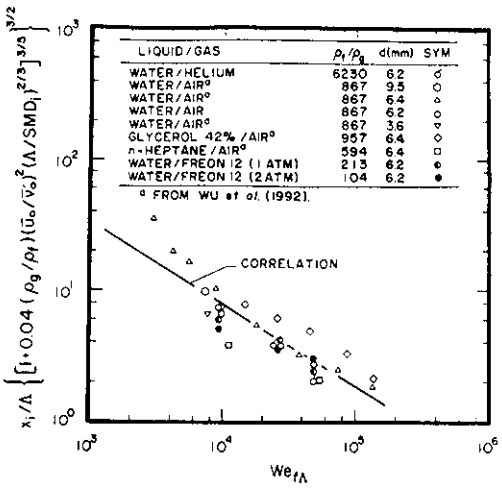

Fig. 6 Length to initiate aerodynamically-enhanced turbulent primary breakup as a function of $We_{f\Lambda}$. The correlation is from Eq. (10).

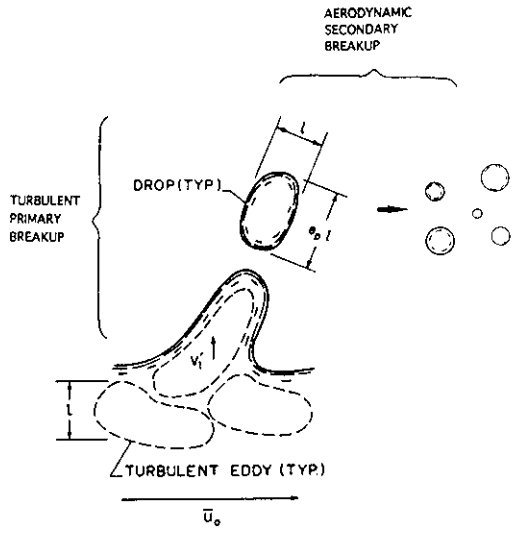

Fig. 7 Sketch of merged turbulent primary- and secondary-breakup at the liquid surface.

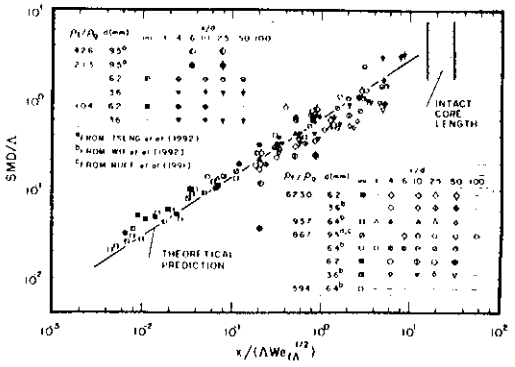

Fig. 9 SMD after turbulent primary breakup as a function of distance from the jet exit after inverting merged secondary breakup effects. Theoretical prediction from Eq. (18).

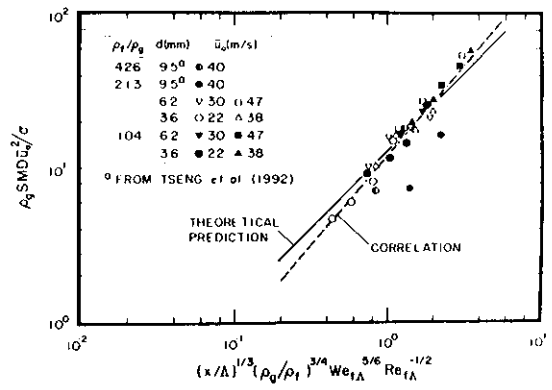

Fig. 8 SMD after aerodynamically-enhanced turbulent primary breakup as a function of distance from the jet exit. Theoretical prediction from Eq. (17), correlation from Eq. (16).

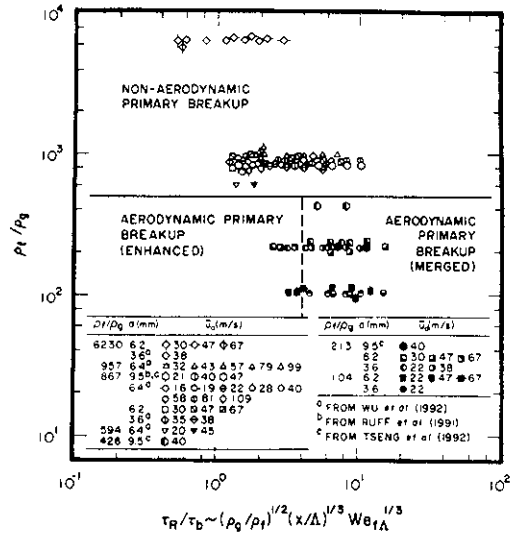

Fig. 10 Turbulent primary breakup regime map.